



Cite this: *Polym. Chem.*, 2014, 5, 6718

Nonvolatile transistor memory devices based on high-*k* electrets of polyimide/TiO₂ hybrids†

Ying-Hsuan Chou,‡^a Chia-Liang Tsai,‡^b Wen-Chang Chen*^{a,b} and Guey-Sheng Liou*^b

Novel nonvolatile memory behaviors of n-type *N,N'*-bis(2-phenylethyl)-perylene-3,4,9,10-tetracarboxylic diimide (BPE-PTCDI) based organic field-effect transistors (OFET) using the new polyimides (PIs), (poly[9,9-bis(4-(4-amino-3-hydroxyphenoxy)phenyl)fluorene-oxydiphthalimide]) **PI(F-ODPA)** and (poly[4,4'-bis(4-amino-3-hydroxyphenylthio)diphenyl sulfide-oxydiphthalimide]) **PI(3S-ODPA)**, and their PI/TiO₂ hybrids as electrets are reported. The OFET memory devices derived from **PI(F-ODPA)** with π -conjugated fluorene moieties exhibited a larger memory window (8.6 V), and could be further enhanced by introducing TiO₂ (up to 20 wt%) into the PIs. In addition, PI/TiO₂ hybrids as electrets for memory devices also could effectively reduce the operating voltage, indicating that the charge transfer capability of TiO₂ plays an important role in transferring and storing the charge for OFET memory devices.

Received 12th June 2014,
Accepted 3rd August 2014

DOI: 10.1039/c4py00825a

www.rsc.org/polymers

Introduction

Organic polymeric material based electrical memory devices have the advantages of being low-cost, easily processable, and structurally flexible as compared to inorganic silicon-based devices.^{1–9} Resistor- and transistor-based memory devices are the popular architectural approaches to operate the memory devices. However, organic field effect transistor (OFET) type memory devices have attracted a great deal of attention due to their easily integrating structure, non-destructive reading, and multiple-bit storage in a single transistor.¹⁰ The device configuration for conventional transistors consisted of an additional polymer dielectric layer (referred to as a polymer electret) between a semiconductor layer and a gate contact. Polymer electrets are dielectric materials with a long-term charge storing ability or electrostatic polarization, including the chargeable polymer electret,^{11,12} organic ferroelectric oriented-dipole dielectric materials,^{13,14} and nanoparticle (NP) embedded or nanostructured gate dielectrics.^{15–17} Kim and co-workers described that the charge trapping ability of the poly(α -methyl styrene) electret could induce memory characteristics of the pentacene-based OFET device.¹² They also demon-

strated that the hydrophilicity and dielectric polarity of polymer electrets significantly affected the device performance.¹⁸ Recently, the pentacene-based transistors with non-volatile flash memory characteristics using the polymer electrets containing different pendent conjugation lengths were also reported.¹⁹

Polyimides (PIs) have been widely explored for applications in flexible organic electronics, such as light-emitting materials,²⁰ photovoltaics,²¹ xerography,²² resistor-type memory,^{23–26} and OFETs,^{27,28} due to their excellent electrical properties, thermal stability, and chemical resistance. The mechanism of resistive-type memory devices could be ascribed to the donor-acceptor (D-A) intramolecular charge transfer (ICT) from the PIs under an applied electric field.^{29–33} Recently, we also reported that the intensity of charge transfer in D-A PI electrets, poly[2,5-bis(4-aminophenylsulfanyl)-selenophene-hexafluoroisopropylidenedipthalimide] (**PI(APSP-6FDA)**) and poly[2,5-bis(4-aminophenylsulfanyl)-thiophene-hexafluoroisopropylidenedipthalimide] (**PI(APST-6FDA)**), could significantly affect the memory window of n-type BPE-PTCDI-based OFET memory devices.³⁴ Furthermore, the OFET devices derived from triphenylamine-based PI electrets with higher dielectric constant (*k*) were also fabricated and they demonstrated an enhanced capability for storing the charges.³⁵

In fact, one of the major challenges in the development of OFETs is rather high voltage needed to operate when using organic gate dielectrics, making these devices impractical for low-priced applications. The key to low-voltage application resides in the reduction of the threshold voltage and the inverse sub-threshold slope. Both parameters are basically

^aDepartment of Chemical Engineering, National Taiwan University, Taipei, Taiwan 10617

^bInstitute of Polymer Science and Engineering, National Taiwan University, Taipei, Taiwan 10617. E-mail: gsliau@ntu.edu.tw, chemwc@ntu.edu.tw

† Electronic supplementary information (ESI) available: Tables: inherent viscosities, molecular weights, and solubility of the polyimides. Figures: ¹H NMR spectrum and contact angles of the PIs, AFM topographies of the PIs and their PI/TiO₂ hybrid electrets. See DOI: 10.1039/c4py00825a

‡ These authors contributed equally to this work.

controlled by the gate insulator. Therefore, using high-*k* hybrid electrets might be a promising approach to operate the devices at low voltages. Manipulation of the dielectric layer could be accomplished using inorganic/organic hybrid dielectric materials due to their robust insulating properties and the ease of processing. By introducing PI into the hybrid materials not only could obtain tough and good quality electret films *via* solution-processable casting or spin coating but also preserve the advantages and characteristics of high breakdown strength, flexibility, and high mechanical strength in these hybrid materials. This approach combines the advantages including high permittivity of the inorganic inclusions, and high breakdown strength, mechanical flexibility, and easy processability of the organic counterparts. Lee *et al.*³⁶ reported that the performance of the OFET device could be improved significantly when a high-*k* PI hybrid was used as a gate dielectric by blending different concentrations of polyester-modified TiO₂ nanoparticles into a PI matrix. However, one of the principal drawbacks of hybrid films that limits their use in OFETs is high leakage current. A sol-gel technique for the preparation of TiO₂ particles was used to suppress the leakage current of devices, and TiO₂ particles were obtained with nano-scale domain size, narrow particle distribution, and excellent dispersion over the polymer matrix.

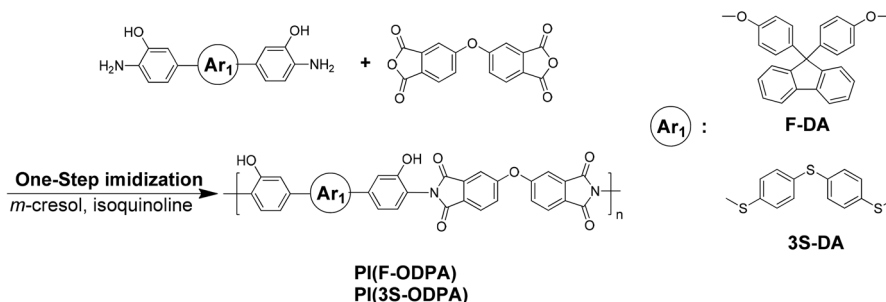
In this study, two new organo-soluble donor-acceptor (D-A) polyimide electrets, **PI(F-ODPA)** and **PI(3S-ODPA)**, with a hydroxyl group on each repeating unit, were synthesized as shown in Scheme 1, and the optical absorption, dielectric con-

stant, and electrochemical properties were described. Furthermore, the PI hybrid gate dielectrics with various contents of TiO₂ (*k* = 48 for anatase) were prepared by the sol-gel technique. The OFET memory devices with the configuration of *n* + Si/PI-TiO₂ hybrid/BPE-PTCDI/Au were fabricated and operated at low gate voltage, and the most common gate dielectric SiO₂ layer was replaced by the high-*k* PI hybrid electrets to elucidate the effect of the high-*k* hybrid electrets on electrical properties of the OFET memory devices.

Results and discussion

Polymer synthesis and basic properties

New organo-soluble polyimides, **PI(F-ODPA)** and **PI(3S-ODPA)**, with a hydroxyl group on each repeating unit, were synthesized *via* a one-step procedure from fluorene- and sulfide-containing diamines with dianhydride (**ODPA**) in the presence of a catalytic amount of isoquinoline at room temperature for 5 h and at 170–180 °C for 20 h as shown in Scheme 1. The polymerization proceeded homogeneously throughout the procedure and afforded clear and viscous polymer solutions. All the polymers precipitated in a white fiber-like form in high yields when slowly pouring the resulting polymer solutions into methanol. The formation of **PI(F-ODPA)** and **PI(3S-ODPA)** was confirmed by NMR and FT-IR spectroscopy, respectively. The typical ¹H NMR spectrum of **PI(F-ODPA)** is shown in Fig. 1; (DMSO-*d*₆, δ, ppm): 6.47 (d, 4H), 6.98 (d, 4H), 7.16 (m, 6H),



Scheme 1 Synthesis of hydroxyl group-containing polyimides.

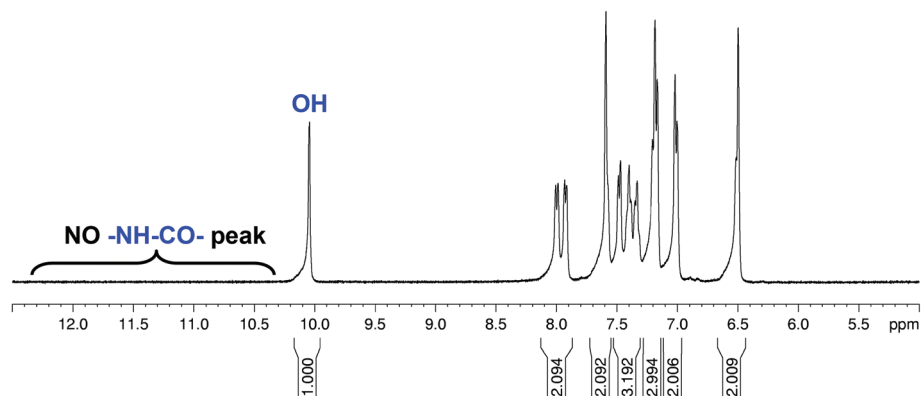


Fig. 1 ¹H NMR spectrum of polyimide **PI(F-ODPA)**.

7.33 (m, 6H), 7.56 (s, 2H), 7.89 (d, 4H), 7.97 (d, 2H), and 10.02 (s, 2H, OH), and the ^1H NMR spectrum of **PI(3S-ODPA)** is added in Fig. S1.† (DMSO- d_6 , δ , ppm): 6.80 (m, 4H), 7.31 (m, 10H), 7.57 (d, 2H), 7.73 (d, 2H), 7.97 (d, 2H) and 10.11 (s, 2H, OH). The inherent viscosities in the range of 0.45–0.72 dL g $^{-1}$ (measured at a concentration of 0.5 g dL $^{-1}$ in DMAc at 30 °C) and solubility behavior of the obtained PIs are listed in Table S1.† The PIs were readily soluble in polar aprotic organic solvents such as DMAc and DMF, and could be solution-casting into flexible, transparent, and tough films. Thus, these novel high performance thin films could be prepared by spin-coating or inkjet-printing processes for practical applications.

Preparation of the polyimide-TiO $_2$ hybrid films

The flexible, transparent, and homogeneous PI/TiO $_2$ hybrid optical films with different titania contents could be successfully prepared. The procedure of the polyimide-TiO $_2$ hybrid with 20 wt% TiO $_2$ was used as an example to illustrate the general synthetic route used to produce the hybrids. Firstly, 0.05 g (0.060 mmol) of **PI(F-ODPA)** was dissolved in 3 ml of DMAc, and 0.03 g (37 wt%) of HCl was added slowly to the PI solution and stirred at room temperature for 0.5 h. Then, 0.053 ml (0.160 mmol) of Ti(OBu) $_4$ dispersed in 0.053 ml of *n*-butanol was added drop-wise to the above solution with a syringe, and the mixture was stirred at room temperature for further 1 hour. The resulting precursor solution was then filtered through a 0.45 μm PTFE filter before spin-coated onto an ITO glass plate or wafer at 1000–2000 rpm for 60 seconds. The obtained film was treated by the multi-step heating process of 100, 150, 250 °C for 20 min, and 350 °C for 60 min, respectively. The FTIR spectra (Fig. 2) of **PI(F-ODPA)** and the PI/TiO $_2$ (5–50 wt%) hybrid films show a broad absorption band in the region 2500–3700 cm $^{-1}$ (O–H stretch) and characteristic imide absorption bands at 1778 cm $^{-1}$ (asym. C=O str.), 1721 cm $^{-1}$ (sym. C=O str.), 1389 cm $^{-1}$ (C–N), and 747 cm $^{-1}$ (imide ring deformation), respectively. In addition, the Ti–O–Ti band

could also be observed at 650–800 cm $^{-1}$, which is also similar to the previous report.^{37–39}

Optical and electrochemical properties of PIs

Fig. 3(a) shows the optical absorption spectra of **PI(F-ODPA)** and **PI(3S-ODPA)** films on quartz substrates. The band gaps of **PI(F-ODPA)** and **PI(3S-ODPA)** estimated from the onset of the absorption spectra are 3.8 and 3.5 eV, respectively. The typical cyclic voltammograms for the PI electrets are shown in Fig. 3(b), revealing the onset oxidations ($E_{\text{onset}}^{\text{ox}}$) of **PI(F-ODPA)** and **PI(3S-ODPA)** at 1.66 and 1.27 V versus Ag/Ag $^+$. The highest occupied molecular orbital (HOMO) energy levels of the PI electrets were calculated from the onset of oxidation waves in CV with reference to ferrocene (4.8 eV) using the following equation: $\text{HOMO} = -[E_{\text{onset}}^{\text{ox}} - E_{1/2}^{\text{ferrocene}} + 4.8]\text{eV}$. Besides, the lowest unoccupied molecular orbital (LUMO) energy levels were estimated from the difference between the optical band gap and the HOMO level.⁴⁰ The HOMO levels of **PI(F-ODPA)** and **PI(3S-ODPA)** are –6.01 and –5.71 eV, respectively. The difference of the energy barrier between **PI(F-ODPA)** and BPE-PTCDI was only 0.1 eV as shown in Fig. 4, which may result in higher charge transfer from BPE-PTCDI to **PI(F-ODPA)**.

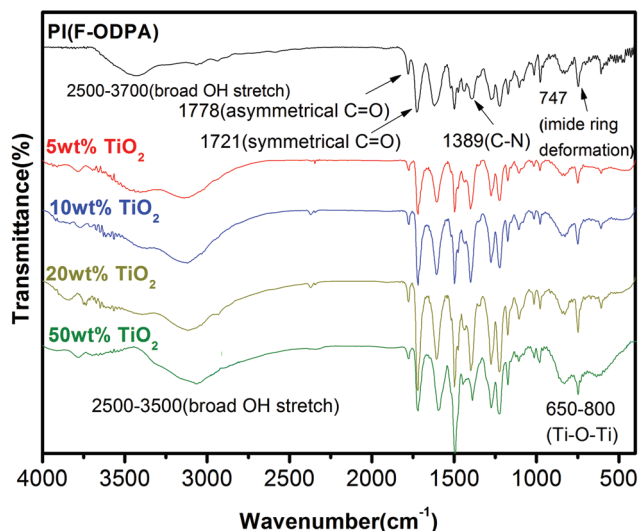


Fig. 2 FT-IR spectra of the studied films **PI(F-ODPA)** and TiO $_2$ hybrid.

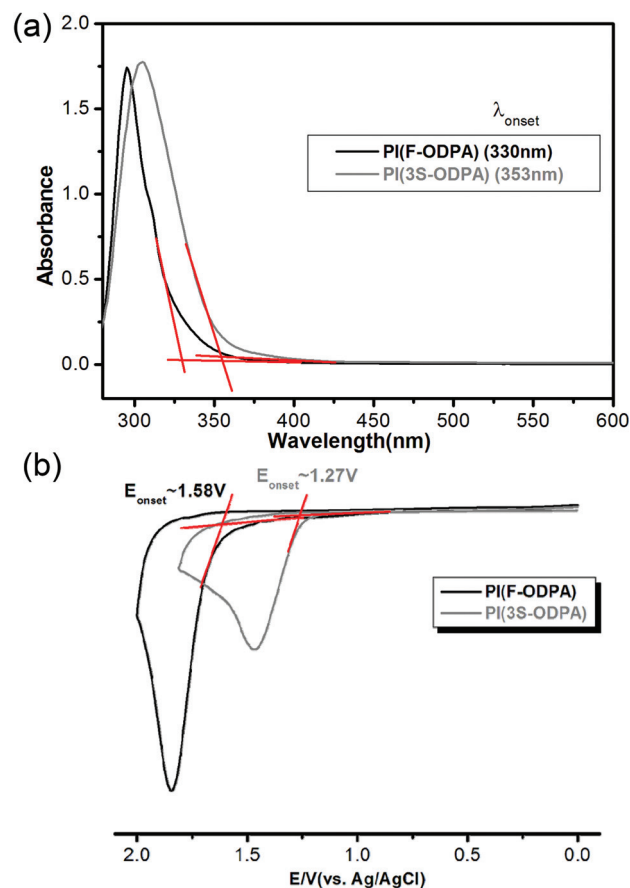


Fig. 3 (a) UV-vis absorption spectra of the prepared PIs on the quartz substrate. (b) Cyclic voltammograms of PI films on ITO-coated glass substrates in 0.1 M TBAP/CH $_3$ CN at a scan rate of 50 mV s $^{-1}$.

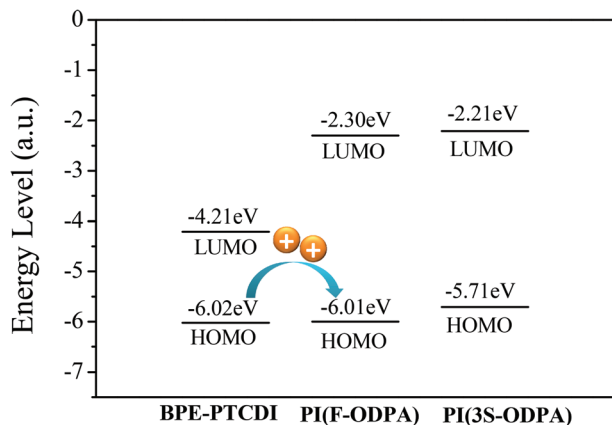


Fig. 4 Energy level diagram of PI(F-ODPA) and PI(3S-ODPA).

Surface morphology characterization

The TEM images (Fig. 5) reveal that the TiO_2 particles were well distributed in PIs by the sol-gel technique with an average size of 5 nm. The morphology of the PI/ TiO_2 hybrid gate dielectric films prepared by spin coating on Si wafer substrates shows a smooth surface with a small root-mean-square value of 0.2–0.6 nm even at a high content of TiO_2 (20 wt%) as shown in the AFM images (Fig. S2 and S3†). In addition, water contact angles for PI(F-ODPA) and PI(3S-ODPA) surfaces were 91° and 72° (Fig. S4†), respectively, implying non-polar and hydrophobic characteristics, and also indicating that PI(F-ODPA) possesses the smaller surface energy between the two PIs. The surface structure of BPE-PTCDI on the PIs was characterized by AFM shown in Fig. 6, and the BPE-PTCDI OFET memory behavior should be mainly attributed to the chemical nature of the BPE-PTCDI and polymer electrets, since the surface roughness of the polymer electrets is similar.⁴¹ The grain sizes of BPE-PTCDI grown on the PI(F-ODPA) and PI(3S-ODPA) surfaces are 193 and 116 nm, respectively. The larger grain size on PI(F-ODPA) could be ascribed to the lower surface energy of PI(F-ODPA), allowing better inter-connection between grains during BPE-PTCDI deposition.⁴²

OFET and memory characteristics

Effect of the PIs as electrets on the OFET memory performance. The memory characteristics of OFET memory devices prepared from the target PIs and their PI/ TiO_2 hybrid electrets were investigated with the bottom-gate/top-contact configuration using n-type BPE-PTCDI as the charge transport layer, as shown in Fig. 7. The transfer characteristics of the OFET devices using PI and TiO_2 hybrids as electrets are depicted in Fig. 8, exhibiting a typical n-type accumulation mode. The field-effect mobility was estimated from the plot of the square root of the drain-to-source current ($I_{\text{ds}})^{1/2}$ versus the gate voltage (V_{g}) by the following equation in the saturation regime:⁴³

$$I_{\text{ds}} = \frac{WC_{\text{poly}}\mu}{2L} (V_{\text{g}} - V_{\text{Th}})^2$$

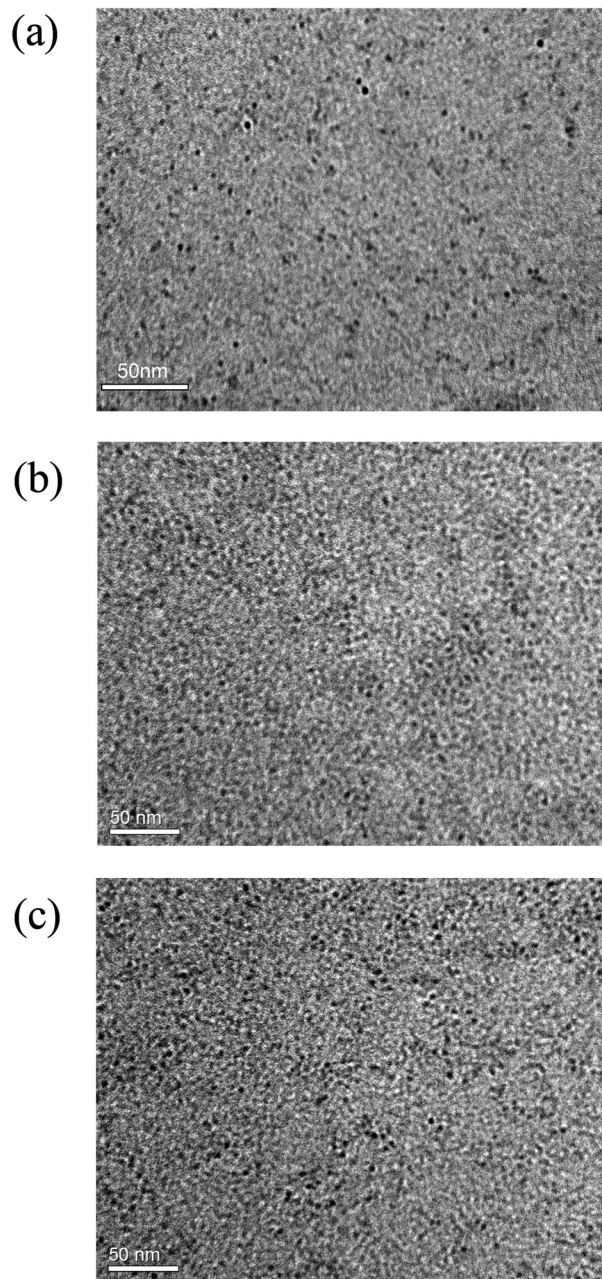


Fig. 5 TEM images of the PI hybrids with (a) 5 wt%, (b) 10 wt%, and (c) 20 wt% TiO_2 contents.

where μ is the field-effect mobility, C_{poly} is the gate dielectric capacitance per unit area and V_{Th} denotes the threshold voltage. The V_{Th} was estimated from the x -axis intercept of the linear section of the plot of V_{g} vs. $(I_{\text{ds}})^{1/2}$. The capacitances (C_{p}) of the gate dielectrics of PI(F-ODPA) and PI(3S-ODPA) measured at 10 kHz were 11.60 and 12.10 nF cm^{-2} , respectively, and the relationship between the capacitance (C_{p}) and the dielectric constant (ϵ) of the polymer electrets is defined as follows:

$$C_{\text{poly}} = \frac{\epsilon_0 \epsilon}{d}$$

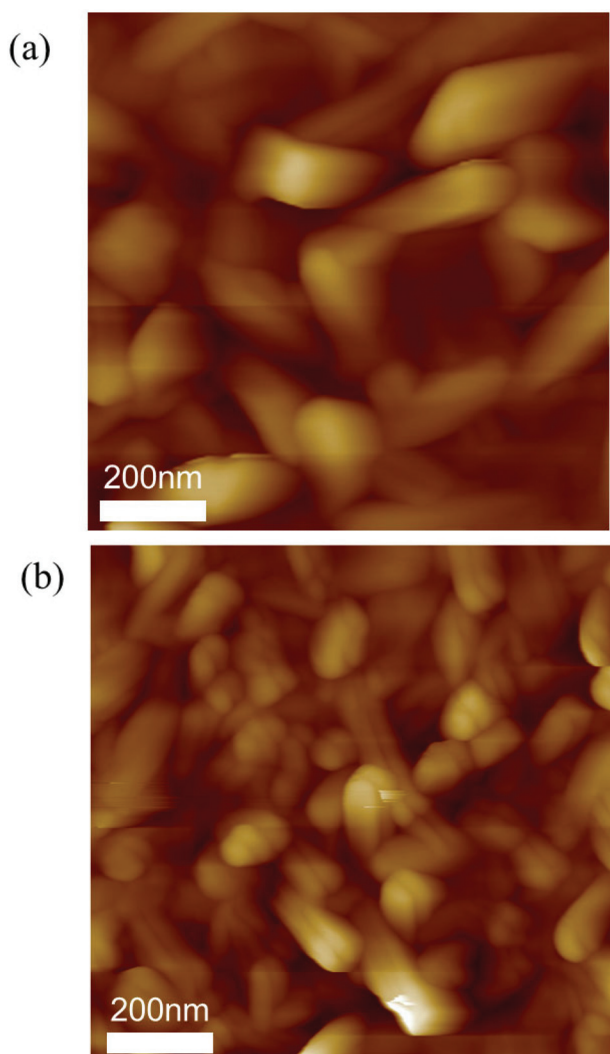


Fig. 6 AFM topographic images of BPE-PTCDI on different PI surfaces: (a) PI(F-ODPA) and (b) PI(3S-ODPA) on $1 \mu\text{m} \times 1 \mu\text{m}$ area.

where ϵ_0 and d are the vacuum permittivity and the insulator thickness. The dielectric constants of PI(F-ODPA) and PI(3S-ODPA) estimated from the measured capacitances were 2.62 and 2.73, respectively.

The characteristics of these BPE-PTCDI-based OFET memory devices are summarized in Table 1. The mobility of the device with PI(F-ODPA) is higher than that with PI(3S-ODPA) as an electret. It is also consistent with the grain size of BPE-PTCDI on the two PIs, ascribed to the more hydrophobic PI(F-ODPA) characteristic that ensures the better wetting and well-formed growth of BPE-PTCDI on the smooth PI(F-ODPA) electret surface. The larger grain sizes and reduced grain boundaries generally result in higher charge-carrier mobility.^{44–46} Furthermore, the interfacial roughness may reduce the mobility due to charge scattering and thus affect the OFET mobility.⁴⁷ The roughness of the PI spin-coated films on bare SiO₂ substrates is 0.175 and 0.235 nm for PI(F-ODPA) and PI(3S-ODPA), respectively (Fig. S2 and S3†). These results reveal that the larger grain size of BPE-PTCDI

and the small roughness of the PI electret surface could contribute to the high-mobility OFET-type memory device. The threshold voltages (V_{Th}) and $I_{\text{on}}/I_{\text{off}}$ current ratios ranging from 1 to 2.2 V and 1.1×10^3 to 3.2×10^3 , respectively, are also summarized in Table 1.

In order to evaluate the memory performance, the device was operated by applying the gate pulse (± 10 V) for one second to cause the shifts of the transfer curves. It thus resulted in the high- (ON state) and low-conductance (OFF state) states under zero gate bias conditions ($V_g = 0$ V). When applying a negative gate bias ($V_g = -10$ V for 1 s), the transfer curves were substantially shifted to the negative direction served as the writing process, leading to a high drain current (ON state) at $V_g = 0$ V. When applied a reverse gate bias ($V_g = 10$ V for 1 s), the transfer curve shifted to the positive direction served as the erasing process. Note that the shift range of the transfer curves through applying a writing and erasing gate bias is defined as the memory windows. The transfer curves of the OFET memory devices based on PI(F-ODPA) and PI(3S-ODPA) with different amounts of TiO₂ as electrets are shown in Fig. 8. On applying a negative gate pulse (writing process), a large amount of positive charges is induced through BPE-PTCDI from the source/drain electrode and then transfer to the HOMO levels of the PI electrets. The negative charges of BPE-PTCDI are easily accumulated at the interface between the BPE-PTCDI and PI electrets due to a built-in electric field induced from retained positive charges, even after removing the external gate voltages. Generally, the D–A PIs could enhance the charge storage through the induced intramolecular charge transfer (ICT) from the donor to the acceptor moiety under an applied voltage. However, the memory windows of the device with PI(F-ODPA) as the electret are larger than PI(3S-ODPA) which probably could be ascribed to the PI(F-ODPA) with the very low HOMO energy barrier (around 0.1 eV), thus facilitating hole transfer from BPE-PTCDI to PI(F-ODPA) and leading to a larger negative shift of the threshold voltage. On the other hand, the interaction between the fluorene groups of PI(F-ODPA) with BPE-PTCDI could facilitate charge trapping in the dielectric–semiconductor interface, resulting in a large V_{Th} shift. We recently demonstrated that the effect on the memory windows of pentacene OFET was proportional to the conjugated fluorene length of polymer electrets.⁴⁸ This indicated that the PI(F-ODPA) with a conjugated fluorene moiety could enhance the charge trapping ability.

Effect of the amount of TiO₂ on the OFET memory performance. Fig. 9(a) and (b) depict the shifts in transfer curves for the memory devices with PI(F-ODPA) as the electret without TiO₂ operated by applying a gate bias of ± 10 V and ± 100 V, respectively. The transfer curves are almost the same with only a little shift in the case of ± 10 V, while the device operated by applying a gate pulse (± 100 V) reveals a much larger memory window. In addition, the memory devices obtained from PI(F-ODPA) hybrids with 5 wt% and 20 wt% of the TiO₂ content as electrets by applying a gate bias of only ± 10 V were also investigated, and the shifts in transfer curves are depicted

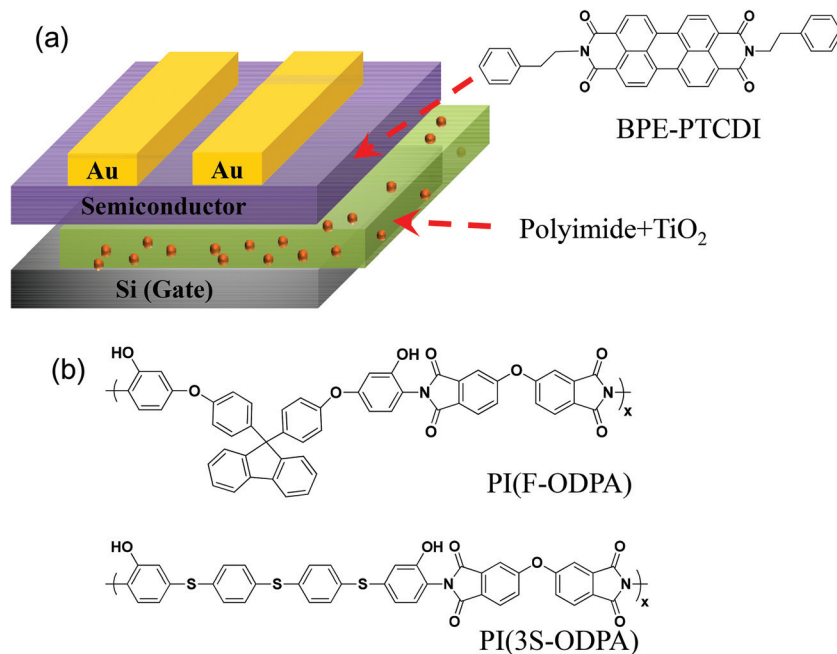


Fig. 7 (a) Schematic structure of the BPE-PTCDI based OFET memory device. (b) Chemical structures of the PI dielectrics.

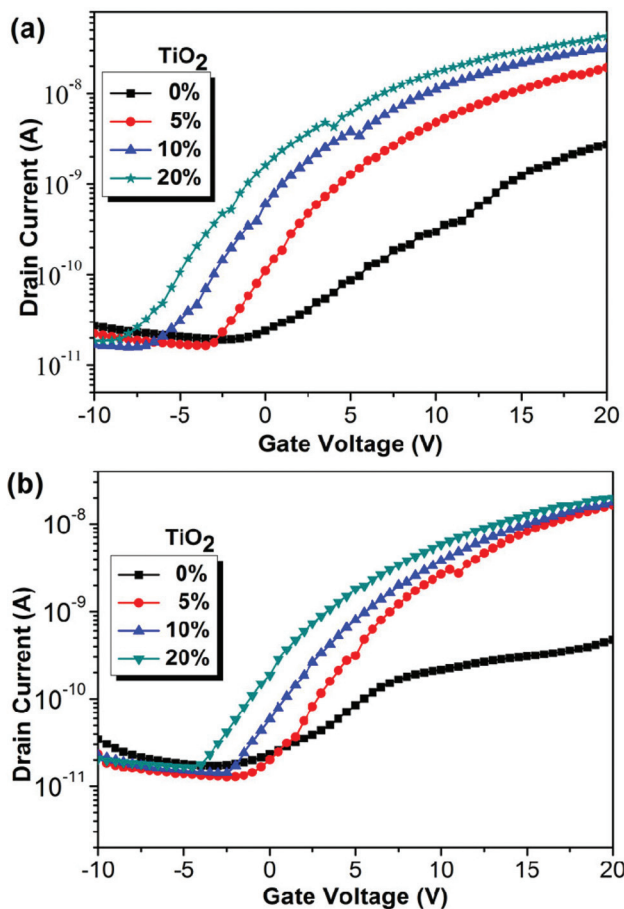


Fig. 8 Shifts in transfer writing curves for BPE-PTCDI OFET memory devices of (a) PI(F-ODPA) and (b) PI(3S-ODPA) with different amounts of TiO₂ as electrets.

Table 1 Characteristics of OFET memory devices with PI/TiO₂ electrets

Polyimide	TiO ₂ (wt%)	Mobility (cm ² V ⁻¹ s ⁻¹)	On/off	V _{Th} (V)	Memory window (V)
PI(F-ODPA)	0	2.1 × 10 ⁻³	1.1 × 10 ³	1.1	2.1
	5	2.6 × 10 ⁻³	1.6 × 10 ³	1.4	3.0
	10	3.2 × 10 ⁻³	2.1 × 10 ³	1.8	7.2
PI(3S-ODPA)	20	4.3 × 10 ⁻³	3.2 × 10 ³	2.0	8.6
	0	9.2 × 10 ⁻⁴	8.6 × 10 ²	1.2	1.8
	5	1.1 × 10 ⁻³	9.2 × 10 ²	1.5	2.2
	10	1.5 × 10 ⁻³	1.1 × 10 ³	1.7	5.3
	20	3 × 10 ⁻³	1.8 × 10 ³	2.1	6.1

in Fig. 10. The memory window enlarges with the increasing content of TiO₂, indicating that the TiO₂ added into the PI as electrets could effectively reduce the operating voltage of the prepared memory devices. The device prepared from the PI(F-ODPA) hybrid with TiO₂ (20 wt%) as the electret exhibited a memory window of up to 8.6 V. Fig. 11 shows the optical absorption spectra of PIs and their hybrid films on quartz substrates. Polyimides with an increased amount of TiO₂ exhibit apparently the absorption intensity in the wavelength above 360 nm. It implies that the addition of TiO₂ into D-A PIs could enhance the charge storage through the induced intramolecular charge transfer from the donor to the acceptor moiety,^{49,50} which probably relates to the electron-donating characteristics of the PI-TiO₂.

Moreover, the dielectric constants of the PI/TiO₂ hybrid gate dielectric samples with different TiO₂ contents were measured at 10 kHz. The obtained dielectric constant increases with increasing TiO₂ content in PI ranging from 2.62 to 13.50 as summarized in Fig. 12, indicating that nano-TiO₂ particles could effectively increase the dielectric constant

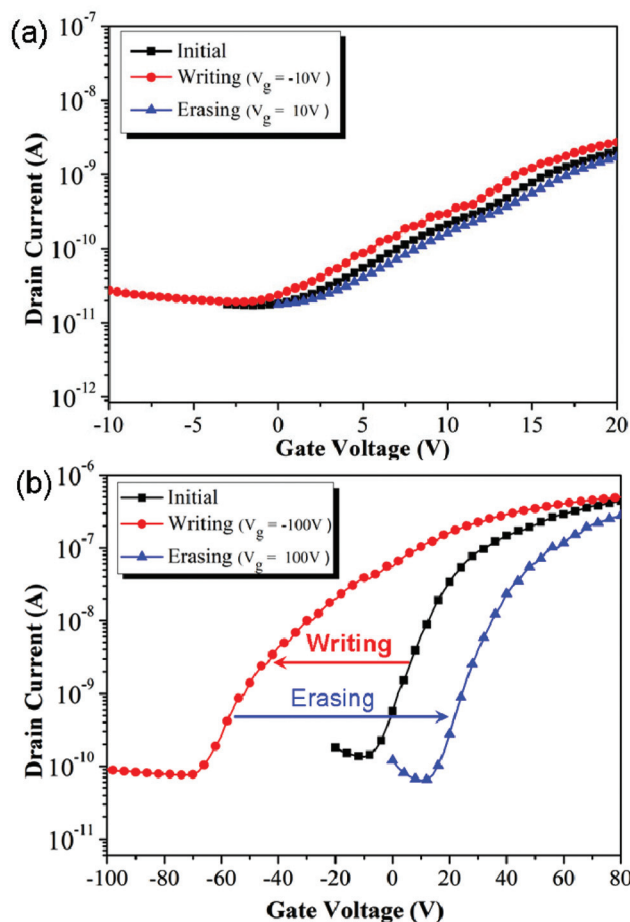


Fig. 9 Shifts in transfer curves for BPE-PTCDI OFET memory devices of PI(F-ODPA) as electrets and with different applied gate biases (a) ± 10 V and (b) ± 100 V.

because nano-TiO₂ particles have a relatively high dielectric constant. Compared to the bare 100 nm thick SiO₂ wafer with a capacitance of 34.5 nF cm⁻², the capacitances of the PIs with the higher amount of nano-TiO₂ (20 wt%) remarkably increase as summarized in Table 2. The higher dielectric constant of the PI hybrids allows the devices to operate in a voltage range below 10 V. To gain more insight into the effect of the nano-composite on the devices, n-type BPE-PTCDI based transistor memory devices using the bare 100 nm thick SiO₂ wafer as a dielectric layer were fabricated for comparison (Fig. S5[†]). As estimated from Fig. S5[†], the BPE-PTCDI transistor showed the mobility of 2.1×10^{-3} cm² V⁻¹ s⁻¹ with an ON/OFF ratio of 2.3×10^3 and an initial threshold voltage of 5 V. By applying a negative and positive gate bias for 1 s to write and erase the device, the sweep curves were not significantly varied. It suggests that the PI/TiO₂ hybrid dielectric layers with a higher dielectric constant could lead the device to be operated at lower gate voltage. On the other hand, by increasing the amount of TiO₂ in PIs as the electret could enhance the charge transfer and thus improve the charge trapping ability.

Charge retention time, a critical feature for the reliable memory devices, was also investigated to demonstrate the

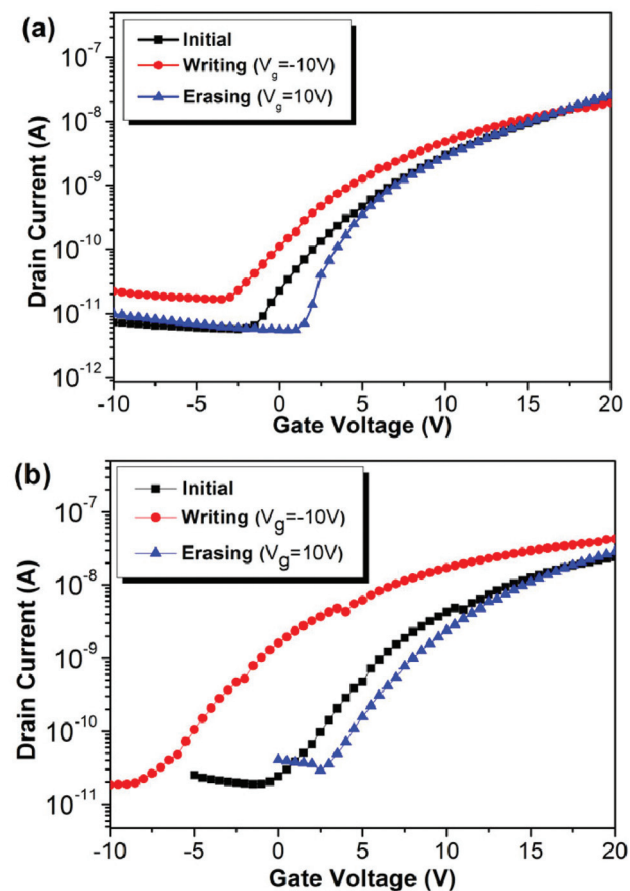


Fig. 10 Shifts in transfer curves for BPE-PTCDI OFET memory devices of PI(F-ODPA) with (a) 5 wt% and (b) 20 wt% of TiO₂ as electrets at ± 10 V applied gate bias.

potential of the target devices. The time duration of the stored charge retained in the dielectric layer is defined as the retention time. The retention times of the BPE-PTCDI-based devices fabricated from PI(F-ODPA) and PI(3S-ODPA) with 20 wt% TiO₂ as the electret are shown in Fig. 13. The stability of the ON and OFF states is maintained for 10⁴ s with ON/OFF current ratios of 10³ and 10² for PI(F-ODPA) and PI(3S-ODPA) with 20 wt% TiO₂, respectively, suggesting good retention properties for nonvolatile memory characteristics. Comparing these two PI hybrid systems, the PI(F-ODPA) with 20 wt% TiO₂ exhibits the superior stability and larger ON/OFF current ratio, which is probably attributed to the stronger charge transfer. The long charge retention time also demonstrates that the OFET memory devices based on D-A PIs with TiO₂ as the electret are promising candidates for nonvolatile memory applications.

Conclusions

Two novel solution-processable D-A polyimides with pendant hydroxyl groups were synthesized. The hydroxyl groups could react with titanium butoxide (Ti(OBu)₄), providing organic-

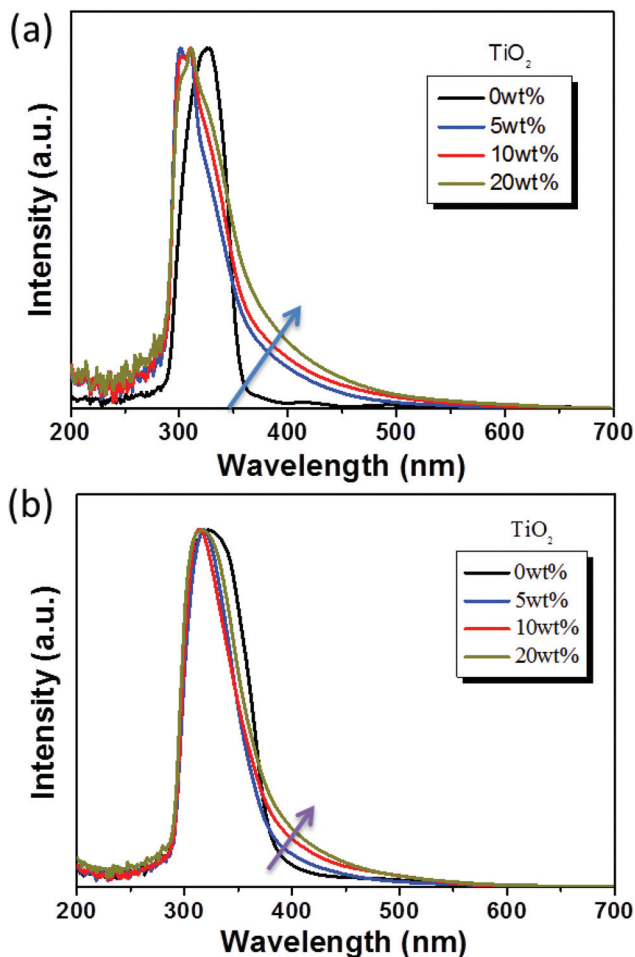


Fig. 11 UV-vis absorption spectra of the PIs: (a) PI(F-ODPA) and (b) PI(3S-ODPA) with TiO₂ on the quartz substrate (thickness: ~150 nm).

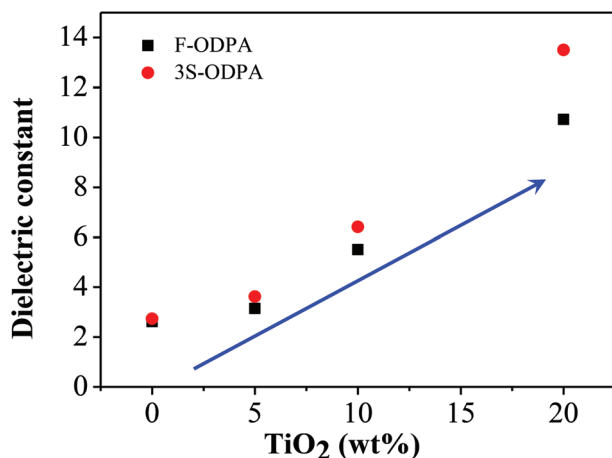


Fig. 12 The relationship between the content of TiO₂ and the dielectric constant.

inorganic bonding sites at each repeating unit with TiO₂ concentrations from 0 wt% to 20 wt% by the sol-gel technique. The BPE-PTCDI OFET memory device based on the PI(F-ODPA)

Table 2 Capacitance and dielectric constants of PI/TiO₂ hybrids

Polyimide	TiO ₂ (wt%)	C _p (nF cm ⁻²)	Dielectric constant (ε _r , at 10 kHz)
PI(F-ODPA)	0	11.60	2.62
	5	13.94	3.15
	10	24.38	5.51
	20	49.93	10.72
PI(3S-ODPA)	0	12.10	2.73
	5	15.26	3.62
	10	27.01	6.41
	20	59.74	13.50
SiO ₂ (100 nm)		34.5	3.9

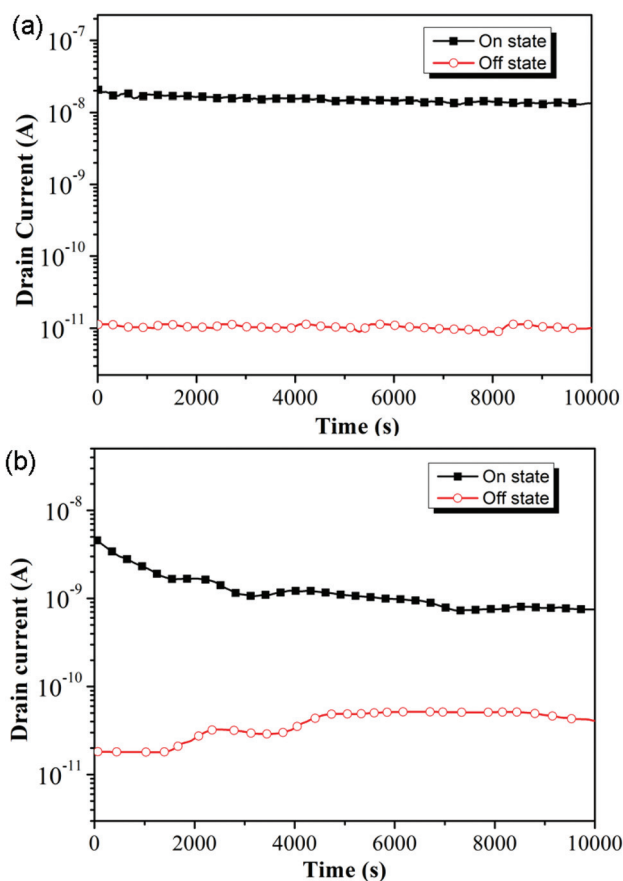


Fig. 13 Retention time testing of the BPE-PTCDI-based OFET memory devices using (a) PI(F-ODPA) and (b) PI(3S-ODPA) with 20 wt% TiO₂ content as the electret.

electret with a conjugated fluorene moiety exhibited the larger memory window compared to PI(3S-ODPA). Moreover, BPE-PTCDI-based OFET nonvolatile memory devices using PI/TiO₂ hybrids with a higher dielectric constant as electrets revealed not only the reducing operating voltage but also the increasing memory window, the ON/OFF ratio, and the stability at ON or OFF states over 10⁴ s. Thus, the novel PI/TiO₂ hybrids with a high dielectric constant as electrets have potential for high performance nonvolatile OFET memory devices.

Experimental section

Materials

Two hydroxyl-containing **PI(F-ODPA)** and **PI(3S-ODPA)** were synthesized from the diamines,³⁷ 9,9-bis(4-(4-amino-3-hydroxyphenoxy)phenyl)fluorene (**F-DA**) and 4,4'-bis(4-amino-3-hydroxyphenylthio)diphenylsulfide (**3S-DA**), with 4,4'-oxydiphthalic dianhydride (**ODPA**) according to the previously reported procedure. *N,N*-Dimethylacetamide (DMAc) (TEDIA), *N,N*-dimethylformamide (DMF) (ACROS), *N*-methyl-2-pyrrolidinone (NMP) (TEDIA), titanium *n*-butoxide (Ti(OBu)₄) (TCI), *n*-butyl alcohol (BuOH) (TCI), and commercially available 4,4'-oxydiphthalic dianhydride (**ODPA**) (TCI) were used as received.

Fabrication of the BPE-PTCDI OFET memory devices

The transistor-type memory devices based on a BPE-PTCDI thin film were fabricated by spin-coating the solutions of **PI(F-ODPA)**, **PI(3S-ODPA)**, and the PI hybrids with different contents of TiO₂ in DMAc at 1000 rpm for 60 s on a highly doped *n*-type Si gate electrode. Then, the thin films were dried under vacuum (10⁻⁶ torr) at 100 °C for 1 h to remove the residual solvent. The thickness of the obtained thin film electrets was controlled at around 65–70 nm. The BPE-PTCDI layer was prepared by thermal deposition with a deposition rate of 0.3–0.4 nm s⁻¹ at 100 °C under vacuum (10⁻⁷ torr) to form a 50 nm thick film. The top-contact source and drain electrodes were defined by 80 nm thick gold through a regular shadow mask, and the channel length (*L*) and width (*W*) were 50 and 1000 μm, respectively. The current–voltage (*I*–*V*) characteristics of the devices were measured using a Keithley 4200-SCS semiconductor parameter analyzer in a N₂-filled glove box.

Characterization

The ¹H NMR spectrum was measured on a Bruker AC-300 MHz spectrometer in DMSO-*d*₆, using tetramethylsilane as an internal reference, and the peak multiplicity was reported as follows: s, singlet; d, doublet; m, multiplet. Fourier transform infrared (FT-IR) spectra were recorded on a PerkinElmer spectrum 100 Model FT-IR spectrometer with a resolution of 1 cm⁻¹ and the number of scans being 4. The inherent viscosity was determined at 0.5 g dL⁻¹ concentration using a Tamson TV-2000 viscometer at 30 °C. Gel permeation chromatographic (GPC) analysis was carried out on a Waters chromatography unit interfaced with a Waters 2410 refractive index detector, calibrating with polystyrene standards. Two Waters 5 μm Styragel HR-2 and HR-4 columns (7.8 mm I.D. × 300 mm) were connected in series with NMP as the eluent at a flow rate of 0.5 ml min⁻¹ at 40 °C. Atomic force microscopy (AFM) measurements were obtained with a NanoScope IIIa AFM at room temperature. Commercial silicon cantilevers with typical spring constants of 21–78 Nm⁻¹ were used to operate the AFM in tapping mode. The morphology of the prepared PI/TiO₂ hybrid films was characterized by transmission electron microscopy (TEM, JEOL 1230). UV–Vis absorption spectra were recorded on a Hitachi U-4100 spectrophotometer. Cyclic voltammetry (CV) was performed with a three-electrode cell in

which ITO, platinum wire, and Ag/AgCl, KCl (sat.) were used as the working electrode, auxiliary electrode, and reference electrode, respectively. The electrochemical properties of the PI films were detected in 0.1 M anhydrous acetonitrile solution containing tetrabutylammonium perchlorate (TBAP) as the electrolyte. The thickness of thin films was measured with a Microfigure measuring instrument (Surfcoorder ET3000, Kosaka Laboratory Ltd). X-ray diffraction (XRD) was performed using a X'Pert PRO X-ray diffractometer using Cu-Kα radiation (λ = 1.5418 Å) with a scan range of 5–30 degrees and 0.2 degrees per step. The electrical characterization of the memory device was performed using a Keithley 4200-SCS semiconductor parameter analyzer in a glove box. For the capacitance measurement, the metal–insulator–semiconductor (MIS) structure was fabricated by depositing gold electrodes on the polymer-coated *n*-type Si (300) wafers. The capacitance of the bilayer dielectrics was measured on the MIS structure using a Keithley 4200-SCS equipped with a digital capacitance meter (model 4210-CVU).

Acknowledgements

We gratefully acknowledge the National Science Council of Taiwan for the financial support.

Notes and references

- 1 Y. Guo, G. Yu and Y. Liu, *Adv. Mater.*, 2010, **22**, 4427–4447.
- 2 W. L. Leong, N. Mathews, B. Tan, S. Vaidyanathan, F. Dotz and S. J. Mhaisalkar, *Mater. Chem.*, 2011, **21**, 5203–5214.
- 3 Q. D. Ling, D. J. Liaw, C. Zhu, D. S. H. Chan, E. T. Kang and K. G. Neoh, *Prog. Polym. Sci.*, 2008, **33**, 917–978.
- 4 J. S. Lee, *J. Mater. Chem.*, 2011, **21**, 14097–14112.
- 5 Y. Yang, J. Ouyang, L. Ma, R. J. H. Tseng and C. W. Chu, *Adv. Funct. Mater.*, 2006, **16**, 1001–1014.
- 6 C. L. Liu and W. C. Chen, *Polym. Chem.*, 2011, **2**, 2169–2174.
- 7 Y. K. Fang, C. L. Liu, C. Li, C. J. Lin, R. Mezzenga and W. C. Chen, *Adv. Funct. Mater.*, 2010, **20**, 3012–3024.
- 8 J. C. Chen, C. L. Liu, Y. S. Sun, S. H. Tung and W. C. Chen, *Soft Matter*, 2012, **8**, 526–535.
- 9 N. G. Kang, B. Cho, B. G. Kang, S. Song, T. Lee and J. S. Lee, *Adv. Mater.*, 2012, **24**, 385–390.
- 10 Y. Guo, C.-a. Di, S. Ye, X. Sun, J. Zheng, Y. Wen, W. Wu, G. Yu and Y. Liu, *Adv. Mater.*, 2009, **21**, 1954–1959.
- 11 H. E. Katz, X. M. Hong, A. Dodabalapur and R. Sarpeshkar, *J. Appl. Phys.*, 2002, **91**, 1572–1576.
- 12 K. J. Baeg, Y. Y. Noh, J. Ghim, S. J. Kang, H. Lee and D. Y. Kim, *Adv. Mater.*, 2006, **18**, 3179–3183.
- 13 R. Schroeder, L. A. Majewski and M. Grell, *Adv. Mater.*, 2004, **16**, 633–636.
- 14 S. H. Lim, A. C. Rastogi and S. B. Desu, *J. Appl. Phys.*, 2004, **96**, 5673–5682.

- 15 W. L. Leong, N. Mathews, S. Mhaisalkar, Y. M. Lam, T. Chen and P. S. Lee, *J. Mater. Chem.*, 2009, **19**, 7354–7361.
- 16 K. J. Baeg, Y. Y. Noh, H. Sirringhaus and D. Y. Kim, *Adv. Funct. Mater.*, 2010, **20**, 224–230.
- 17 M. Burkhardt, A. Jedaa, M. Novak, A. Ebel, K. Voïtchovsky, F. Stellacci, A. Hirsch and M. Halik, *Adv. Mater.*, 2010, **22**, 2525–2528.
- 18 K. J. Baeg, Y. Y. Noh, J. Ghim, B. Lim and D. Y. Kim, *Adv. Funct. Mater.*, 2008, **18**, 3678–3685.
- 19 Y. H. Chou, S. Takasugi, R. Goseki, T. Ishizone and W. C. Chen, *Polym. Chem.*, 2014, **5**, 1063–1071.
- 20 (a) E. I. Mal'tsev, M. A. Brusentseva, D. A. Lypenko, V. I. Berendyaev, V. A. Kolesnikov, B. V. Kotov and A. V. Vannikov, *Polym. Adv. Technol.*, 2000, **11**, 325–329; (b) H. J. Yen and G. S. Liou, *Chem. Commun.*, 2013, **49**, 9797–9799; (c) H. J. Yen, J. H. Wu, W. C. Wang and G. S. Liou, *Adv. Opt. Mater.*, 2013, **1**, 668–676.
- 21 D. Mühlbacher, C. J. Brabec, N. S. Sariciftci, B. V. Kotov, V. I. Berendyaev, B. M. Romyantsev and J. C. Hummelen, *Synth. Met.*, 2001, **121**, 1609–1610.
- 22 Z. Y. Wang, Y. Qi, J. P. Gao, G. G. Sacripante, P. R. Sundararajan and J. D. Duff, *Macromolecules*, 1998, **31**, 2075–2079.
- 23 G. Tian, D. Wu, S. Qi, Z. Wu and X. Wang, *Macromol. Rapid Commun.*, 2011, **32**, 384–389.
- 24 Y. L. Liu, K. L. Wang, G. S. Huang, C. X. Zhu, E. S. Tok, K. G. Neoh and E. T. Kang, *Chem. Mater.*, 2009, **21**, 3391–3399.
- 25 K. L. Wang, Y. L. Liu, I. H. Shih, K. G. Neoh and E. T. Kang, *J. Polym. Sci., Part A: Polym. Chem.*, 2010, **48**, 5790–5800.
- 26 C. L. Liu, T. Kurosawa, A. D. Yu, T. Higashihara, M. Ueda and W. C. Chen, *J. Phys. Chem. C*, 2011, **115**, 5930–5939.
- 27 D. Ji, L. Jiang, Y. Guo, H. Dong, J. Wang, H. Chen, Q. Meng, X. Fu, G. Tian, D. Wu, G. Yu, Y. Liu and W. Hu, *Adv. Funct. Mater.*, 2014, **24**, 3783–3789.
- 28 D. Ji, L. Jiang, X. Cai, H. Dong, Q. Meng, G. Tian, D. Wu, J. Li and W. Hu, *Org. Electron.*, 2013, **14**, 2528–2533.
- 29 N. H. You, C. C. Chueh, C. L. Liu, M. Ueda and W. C. Chen, *Macromolecules*, 2009, **42**, 4456–4463.
- 30 Y. L. Liu, Q. D. Ling, E. T. Kang, K. G. Neoh, D. J. Liaw, K. L. Wang, W. T. Liou, C. X. Zhu and D. S. H. Chan, *J. Appl. Phys.*, 2009, **105**, 044501.
- 31 (a) S. G. Hahm, S. Choi, S. H. Hong, T. J. Lee, S. Park, D. M. Kim, W.-S. Kwon, K. Kim, O. Kim and M. Ree, *Adv. Funct. Mater.*, 2008, **18**, 3276–3282; (b) S. G. Hahm, S. Choi, S. H. Hong, T. J. Lee, S. Park, D. M. Kim, J. C. Kim, W. Kwon, K. Kim, M. J. Kim, O. Kim and M. Ree, *J. Mater. Chem.*, 2009, **19**, 2207–2214; (c) K. Kim, S. Park, S. G. Hahm, T. J. Lee, D. M. Kim, J. C. Kim, W. Kwon, Y. G. Ko and M. Ree, *J. Phys. Chem. B*, 2009, **113**, 9143–9150.
- 32 (a) C. J. Chen, H. J. Yen and G. S. Liou, *J. Mater. Chem. C*, 2013, **1**, 7623–7634; (b) H. J. Yen, C. J. Chen and G. S. Liou, *Adv. Funct. Mater.*, 2013, **23**, 5307–5316.
- 33 (a) Y. Liu, Y. Zhang, Q. Lan, S. Liu, Z. Qin, L. Chen, C. Zhao, Z. Chi, J. Xu and J. Economy, *Chem. Mater.*, 2012, **24**, 1212–1222; (b) L. Shi, H. Ye, W. Liu, G. Tian, S. Qi and D. Wu, *J. Mater. Chem. C*, 2013, **1**, 7387–7399.
- 34 Y. H. Chou, N. H. You, T. Kurosawa, W. Y. Lee, T. Higashihara, M. Ueda and W.-C. Chen, *Macromolecules*, 2012, **45**, 6946–6956.
- 35 Y. H. Chou, H. J. Yen, C. L. Tsai, W. Y. Lee, G. S. Liou and W. C. Chen, *J. Mater. Chem. C.*, 2013, **1**, 3235–3243.
- 36 W. H. Lee, C. C. Wang, W. T. Chen and J. C. Ho, *Jpn. J. Appl. Phys.*, 2008, **47**, 8955–8960.
- 37 H. J. Yen, C. L. Tsai, P. H. Wang and G. S. Liou, *RSC Adv.*, 2013, **3**, 17048–17056.
- 38 G. S. Liou, P. H. Lin, H. J. Yen, Y. Y. Yu, T. W. Tsai and W. C. Chen, *J. Mater. Chem.*, 2010, **20**, 531–536.
- 39 R. Himmelhuber, P. Gangopadhyay, R. A. Norwood, D. A. Loy and N. Peyghambarian, *Opt. Mater. Express*, 2011, **1**, 252–258.
- 40 C. L. Liu, J. C. Hsu, W. C. Chen, K. Sugiyama and A. Hirao, *ACS Appl. Mater. Interfaces*, 2009, **1**, 1974–1979.
- 41 M. H. Yoon, C. Kim, A. Facchetti and T. J. Marks, *J. Am. Chem. Soc.*, 2006, **128**, 12851–12869.
- 42 H. Ma, H. L. Yip, F. Huang and A. K. Y. Jen, *Adv. Funct. Mater.*, 2010, **20**, 1371–1388.
- 43 J. Zaumseil and H. Sirringhaus, *Chem. Rev.*, 2007, **107**, 1296–1323.
- 44 S. Verlaak, V. Arkhipov and P. Heremans, *Appl. Phys. Lett.*, 2003, **82**, 745–747.
- 45 Z. Bao, A. J. Lovinger and A. Dodabalapur, *Appl. Phys. Lett.*, 1996, **69**, 3066–3068.
- 46 L. Torsi, A. Dodabalapur, L. J. Rothberg, A. W. P. Fung and H. E. Katz, *Science*, 1996, **272**, 1462–1464.
- 47 A. I. Kingon, J.-P. Maria and S. K. Streiffer, *Nature*, 2000, **406**, 1032–1038.
- 48 J. C. Hsu, W. Y. Lee, H. C. Wu, K. Sugiyama, A. Hirao and W. C. Chen, *J. Mater. Chem.*, 2012, **22**, 5820–5827.
- 49 C. L. Tsai, C. J. Chen, P. H. Wang and G. S. Liou, *Polym. Chem.*, 2013, **4**, 4570–4573.
- 50 C. J. Chen, C. L. Tsai and G. S. Liou, *J. Mater. Chem. C*, 2014, **2**, 2842–2850.